CONFERENCE PRE-PRINT

COMPREHENSIVE SIMULATIONS OF BURSTING AND NON-BURSTING ALFVÉN WAVES IN ICRF HEATED TOKAMAK PLASMAS

J. WANG, Y. TODO, R. SEKI, H. WANG, M. SATO

National Institute for Fusion Science, National Institutes of Natural Sciences

Toki, Japan

Email: wang.jialei@nifs.ac.jp

A. BIERWAGE

National Institutes for Quantum Science and Technology, Rokkasho Institute for Fusion Energy Aomori, Japan

N. TSUJII

The University of Tokyo

Kashiwa, Japan

Z. CHENG

Zhejiang University

Hangzhou, China

National Institute for Fusion Science, National Institutes of Natural Sciences

Toki, Japan

K. OGAWA

National Institute for Fusion Science, National Institutes of Natural Sciences Toki, Japan The Graduate University for Advanced Studies, SOKENDAI Toki, Japan

Z.X. WANG

Dalian University of Technology

Dalian, China

Abstract

Recurrent bursting Alfvénic instabilities can drastically degrade plasma confinement. Unlike beam-driven shear Alfvén waves (SAWs), which often exhibit bursting behavior, SAWs during ion cyclotron resonance frequency heating (ICRH) typically maintain steady amplitudes, despite theoretical predictions suggesting the possibility of a bursting state. This work reports the first comprehensive simulations of ICRH-driven tokamak plasmas on the slowing-down timescale using the kinetic-MHD hybrid code MEGA, where SAW-induced fast-ion transport is self-consistently included during the high-energy tail formation. Bursting toroidal Alfvén eigenmodes (TAEs) are observed in both multi-n and single-n simulations of plasmas with a relatively low magnetic field ($B_0 = 1.5$ T) and an ICRF resonance layer located at the magnetic axis or on the inboard side, while outboard heating always leads to non-bursting TAEs, where n is the toroidal mode number. The effect of ICRF-driven velocity space diffusion in preventing bursting TAEs is identified in this work, which opens a new avenue for bursting-AE control in burning plasmas through fast-ion phase space engineering via RF waves.

1. INTRODUCTION

The incompressible shear Alfvén waves (SAWs), which can be destabilized via inverse Landau damping by fast particles produced by fusion reactions and auxiliary heating sources such as neutral beam injection (NBI) and/or ion-cyclotron-range-of-frequency (ICRF) heating, are deleterious to the performance of burning plasmas in fusion devices. Various SAW dynamics have been reported in present-day tokamak and stellarator plasmas, which are determined by an interplay between the SAW electric field that flattens the fast ion distribution function and relaxation processes that restore the distribution function. Among those observed SAWs, a beam-driven SAW is often in a 'burst' state accompanied by a rapid and violent release of stored free energy [1-3], such as abrupt large

amplitude events (ALEs) observed in JT-60U [2]. ICRF-induced SAW is typically characterized as a steady state [4-6], but it can also exhibit a periodic modulation state with frequency splitting [7] or a chaotic state [8]. However, ICRF-induced SAW bursts haven't been reported, despite theoretical predictions suggesting the possibility of a bursting state [9-11]. Numerical simulations provide a powerful approach to elucidating the underlying physics in phase space. A series of comprehensive numerical simulations incorporating particle and momentum sources/sinks, as well as collisions, has been conducted to study the nonlinear dynamics of beam-induced modes [12-16]. The results show that the synergetic effects of multiple modes via resonance overlap are responsible for the bursts. However, similar attempts for ICRF-induced SAWs remain unexplored.

In this work, state-of-the-art hybrid particle-in-cell simulations of ICRF-induced toroidal Alfvén eigenmodes (TAEs) in tokamak plasmas are conducted, where both bursting and non-bursting TAEs are reported. To the best of our knowledge, this is the first incorporation of an RF source term into a kinetic-MHD hybrid or gyrokinetic code. Our stability analysis is then performed without making an assumption of minority ion distributions. In Section 2, the extended MEGA model and numerical set-ups will be introduced. In Section 3, both classical simulation and comprehensive simulation results will be presented. We will also show how the ICRF resonance layer position significantly alters the TAE nonlinear dynamics. Section 4 includes concluding remarks and key takeaways.

2. SIMULATION MODEL AND SET-UPS

An extended kinetic-MHD hybrid code MEGA with ICRH is used. Previously, the extended code has successfully predicted ICRF-induced SAWs in the LHD [6]. The extended model includes an ICRF quasilinear operator [17, 18], Coulomb collisions [19], particle sink and source, as well as MHD perturbations. Motions of minority ions described by drift-kinetic equations are simulated using the full-f particle-in-cell (PIC) method, and are coupled to fluid bulk plasma via a current-coupling scheme. Both ICRF acceleration and Coulomb collisions are simulated by the Monte Carlo method. A so-called multi-phase simulation [14] is employed to save computational resources, where a classical simulation (MHD solver off) and a hybrid simulation (MHD solver on) are executed alternately until a steady state, followed by a continuous hybrid simulation till the end. It should be noted that the nonlinear SAW states are defined at a continuous hybrid simulation phase. A TFTR-like plasma equilibrium is used. The major and minor radii are 2.6 m and 0.9m, respectively. The circular outermost magnetic surface is adopted to avoid the interference by elliptical Alfvén eigenmodes (EAEs). The field strength at the magnetic axis is 1.5T. A deuterium plasma with a minority hydrogen ratio 4% is adopted. The central electron density and temperature are $3.0 \times 10^{19} \text{ m}^{-3}$ and 8.0 keV, respectively. A parabolic safety factor profile $q(r/a) = q_0 + (q_a - q_0) \cdot (r/a)^2$ is used, with $q_0=1.2$ and $q_a=3.0$. The shape of the outermost magnetic surface is circular. A modelled ICRF wave electric field profile is adopted for simplicity, with a parallel wave number $k_{\parallel} = 6 \text{ m}^{-1}$. The absorbed RF power is 6 MW, unless otherwise specified. Cylindrical coordinates (R, φ , Z) are employed in MEGA code with a corresponding mesh size of (256, 192, 256). The number of simulation particles is about 0.5 billion.

3. SIMULATION RESULTS

3.1. Classical simulation without shear Alfvén wave relaxation

Figure 1 shows the classical simulation of ICRF heating with the RF resonance layer located near the magnetic axis without any MHD perturbations to relax the minority ion distributions. The absorbed RF power is 6 MW. The minority ions reach a steady state till 350 ms, where the absorbed ICRF power is balanced by the minority ion loss power due to orbit losses and the collisional power from high-energy minority ions to bulk plasmas via Coulomb collisions. In the steady state, drift-motion bounce tips of high-energy minority ions are close to the RF resonance layer, leading to a high minority ion pressure region along the resonance layer in a cross-section with a maximum local beta around 8%. Due to the RF wave kick in perpendicular velocity, the steady state minority ions are highly anisotropic with $v_{\perp} \gg v_{\parallel}$, and a considerable number of minority particles are accelerated to the MeV energy range, as shown in Figure 3(c). The asymmetry of minority ion distribution in v_{\parallel} direction is mainly due to the low magnetic strength ($B_0 = 1.5 \text{ T}$) adopted in this work, which leads to poor fast ion confinement, especially for high-energy particles with $v_{\parallel} < 0$ being kicked at the Doppler-shifted RF resonance layer in the inboard side region of plasma cross-section.

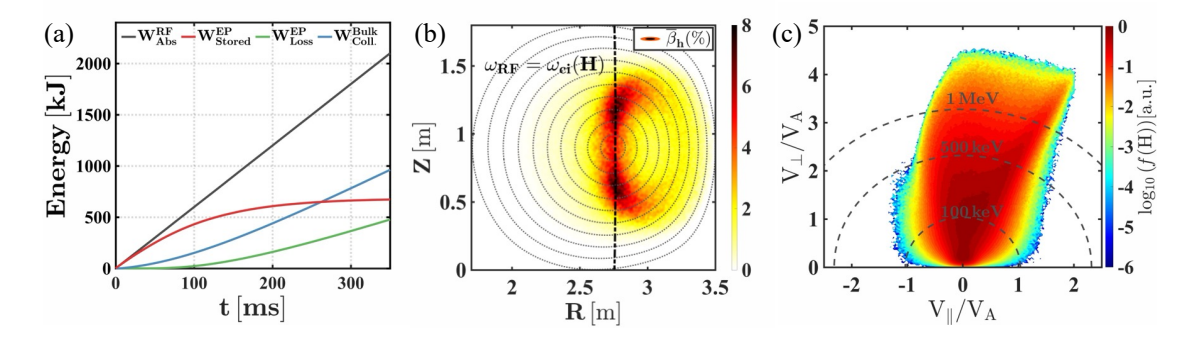


FIG. 1. Classical simulation of on-axis ICRF heating. (a) Evolutions of absorbed RF power, minority ion stored energy, minority ion loss energy, and bulk plasma absorbed energy. (b) Steady-state minority ion beta profile in a cross-section, where the black dashed curve indicates the ICRF resonance layer. (c) Steady-state minority ion velocity space distribution.

3.2. Multi-*n* simulation of bursting shear Alfvén waves

Figure 2 shows the comprehensive simulations of on-axis ICRF heating with multiple toroidal harmonics. In these simulations, dominant harmonics with $n \le 8$ are retained. The multi-phase simulation method is applied with variable time intervals changing from early heating phase [9.5ms classical + 0.5ms hybrid] to later heating phase [1ms classical + 1ms hybrid]. Due to the overshoots in the MHD fluctuations in the multi-phase period, we avoid discussing SAW nonlinear states before the start of the continuous hybrid simulation at 60ms. The recurrent bursting SAWs are observed in the continuous hybrid simulation phase with primary toroidal harmonics $n = 3\sim 6$, and the majority of bursts are governed by n = 3 and n = 4 harmonics. The accessible minority ion beta is drastically decreased to 1.5% compared to the classical simulation result shown in Figure 1. The spatial distribution in a cross-section also significantly differs, where minority ions are transported to the lower field side region by the MHD events. This indicates the necessity of including SAW-induced transport in evaluating ICRH. Minority ions still can be accelerated to the MeV energy range in the comprehensive simulations, and the distribution asymmetry in v_{\parallel} direction is reduced by the regulation of MHD waves. It is worth mentioning that TAEs remain bursting when the ICRF resonance layer is moved to the inboard side.

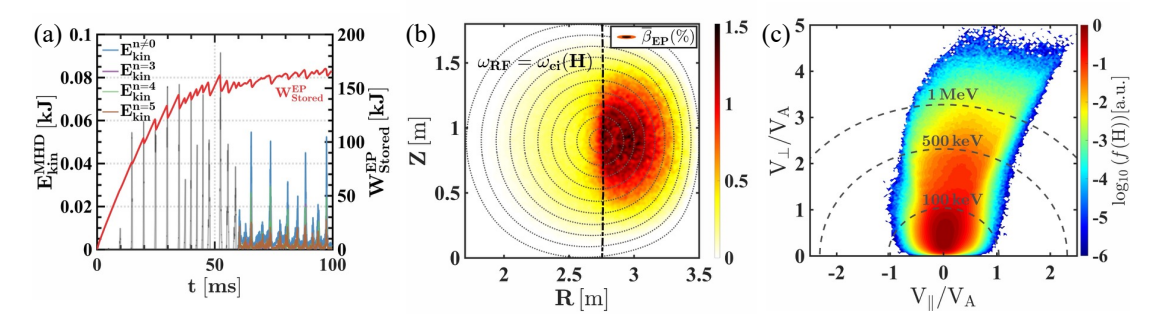


FIG. 2. Multi-phase simulation of ICRF-induced bursting event with an ICRF resonance layer located at the magnetic axis. (a) Evolutions of MHD kinetic energy and minority ion stored energy, where the continuous hybrid simulation starts from 60ms. (b) Steady-state minority ion beta profile at t=96ms in a cross-section. (c) Steady-state minority ion velocity space distribution. The absorbed RF power is 6MW.

Figure 3(a) shows the MHD kinetic energy evolution of one bursting event, which lasts around 1ms. The onset and end time of primary modes are similar, which confirms an interaction between different toroidal mode numbers. However, the strength of this interaction is considerably weaker than the beam-driven burst documented in Refs. [15,16]. For this ICRF-driven burst, each toroidal harmonic exhibits oscillatory growth with alternating distinct growth and decay phases, and the latter is particularly pronounced. For a beam-driven burst [15,16], even when a decay phase occurs for a given mode during one burst, it tends to be short-lived and quickly gives way to the next growth phase due to the strong synergistic multi-*n* effects. Figure 3(b) shows the minority ion beta change by one bursting event, where about 10% minority ions in the core region are transported to the outer region or get lost.

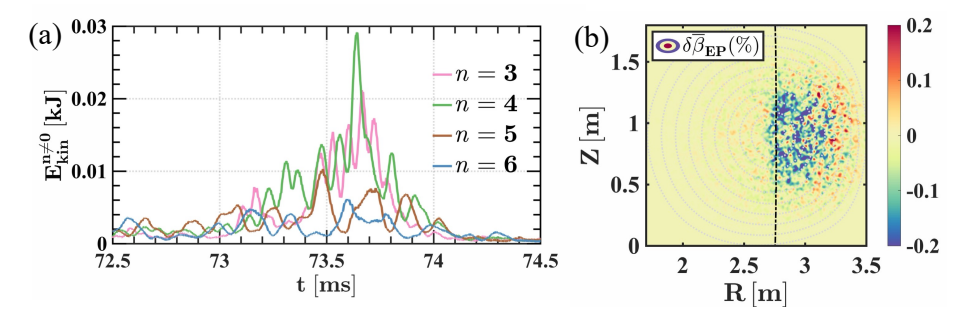


FIG. 3. MHD kinetic energy evolution of one bursting event, which was decomposed into Fourier harmonics with toroidal mode numbers n = 3,4,5,6. (b) Minority ion beta change by the bursting event shown in panel (a).

To clarify the triggering mechanism of the bursting ICRF-induced TAEs, spatial profiles and the frequency spectra for the decomposed toroidal harmonics are analyzed in Figure 4. During the bursting event, a series of discrete TAEs with different frequencies for each toroidal harmonic is formed and there is a spatial overlap region between adjacent TAEs. Time trace of frequency spectrum for those TAEs is shown in Figure 5, where the radial MHD velocity fluctuations are measured at the TAE center with $q_{loc} = (m + 1/2)/n$ on the equatorial plane of the low field at a toroidal angle of $\varphi = 0$. The modes remain non-chirping or very weak chirping behaviour during the burst, which is quite different from the NBI-induced burst with an obvious chirping phenomenon. The resonance condition for fast particles interacting with a low frequency wave (mode frequency much less than the cyclotron frequency) in a torus is $\omega_0 - L\omega_\theta - n\omega_\varphi = 0$, where ω_0 is the mode frequency, and integer L is the resonance number. ω_{θ} and ω_{φ} are particle poloidal and toroidal orbit frequency, respectively. ICRF accelerated minority ions are mainly deeply trapped particles and the resonance condition can be written as $\omega_0 \approx n\omega_d$ with ω_d the bounce-averaged drift frequency, which is proportional to particle kinetic energy and inversely proportional to the flux-averaged safety factor, $\omega_d \propto E/q_{loc}$. It is obvious that radially discrete TAEs of each toroidal harmonic shown in Figure 5 are destabilized by minority ions with a similar energy range, and resonant particles can be radially transported across an extensive region, transferring a substantial amount of energy to the MHD waves. In addition, a similar value of magnetic moment is also an important factor for the resonance overlap, which can be inherently and approximately satisfied in the current scenario. ICRF accelerated steady-state minority ions with similar energies have very close values of magnetic moments, because those particles with similar energies have their bounce tips located around the RF resonance layer before they undergo significant outward transport by SAWs. On the other hand, during the phase of two bursting events, the mode is weak, and radial extension is relatively narrow. The radial distance between two adjacent TAEs provides an environment to accumulate the free energy. Regarding the synergistic effect between different toroidal harmonics, it is noticed that the upper bound of particle energy range for resonating with n = 4 mode approaches the lower bound of those resonating with n=3 mode. The resonance overlap can occur between different toroidal modes for those particles.

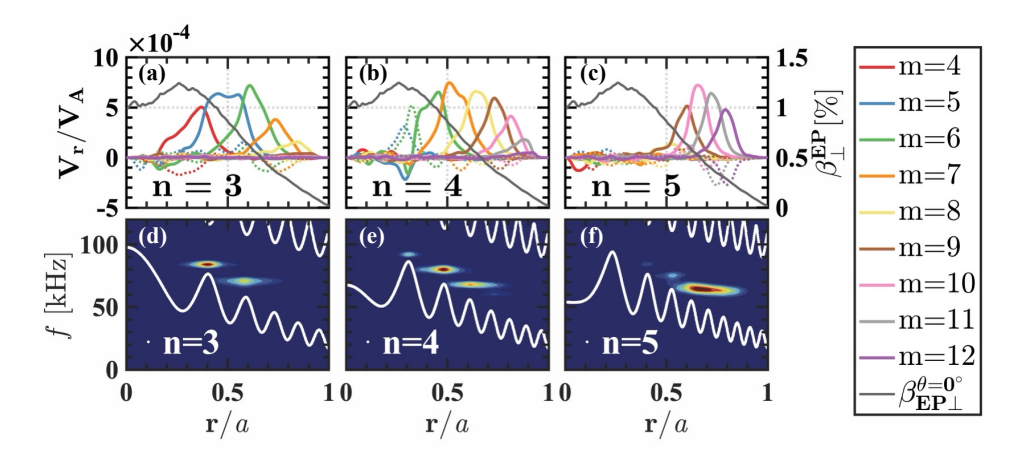


FIG. 4. Spatial profiles and frequency spectra of radial MHD velocity fluctuations at t=73.46ms of the bursting event shown in Fig. 3. Solid (dashed) lines in (a-c) show $cos(m\theta + n\phi)$ [sin $(m\theta + n\phi)$] harmonics with poloidal mode number m listed in the figure. For the spectral analysis, a Hanning time window of width around 0.1ms is used.

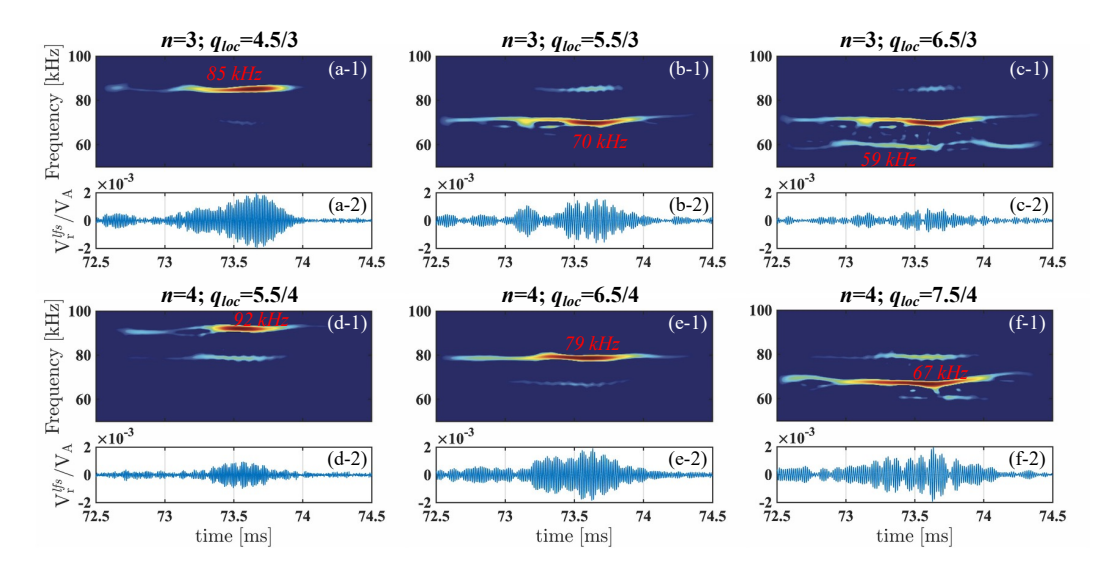


FIG. 5. Time trace of frequency spectrum and radial MHD velocity fluctuations measured at the equatorial plane of the low field side in the cross-section with $\varphi=0$. Panels (a-c) shows the fluctuations for toroidal mode number n=3 at q=(4+1/2)/3 $[r/a\sim0.41]$, q=(5+1/2)/3 $[r/a\sim0.59]$, and q=(6+1/2)/3 $[r/a\sim0.73]$, respectively. Panels (d-f) shows the fluctuations for toroidal mode number n=4 at q=(5+1/2)/4 $[r/a\sim0.31]$, q=(6+1/2)/4 $[r/a\sim0.49]$, and q=(7+1/2)/4 $[r/a\sim0.61]$, respectively.

3.3. Single-*n* simulation of bursting shear Alfvén waves

The weak synergistic effect between different toroidal harmonics in Section 3.2 indicates that TAEs with a single toroidal mode number could also trigger the bursting event. We conducted a single-n comprehensive simulation where only n=3 toroidal mode families are included. In this simulation, n=3 mode is directly driven by fast particles, while n=0,6,9 MHD perturbations are retained, which contribute to the TAE nonlinear saturation [20], especially for the bursting mode with large amplitude.

Recurrent giant bursts are observed during the continuous hybrid phase in Figure 6. Similar to the multi-n case in Figure 3, a series of discrete TAEs with different frequencies is formed, as shown in Figure 6(c). The time interval of two adjacent bursts is longer than that in the multi-n simulation of Figure 3. Then, more free energy is stored in each burst period, and the n=3 MHD kinetic energy during the burst is greater by an order of magnitude than that observed in the multi-n simulation. Figure 6(b) shows the kinetic energy evolution of one burst, which exhibits oscillatory growth. This oscillatory growth results from the different frequencies of inner and outer TAEs, and the fast growth phase corresponds to the in-phase of the TAEs shown in Figure 6(c).

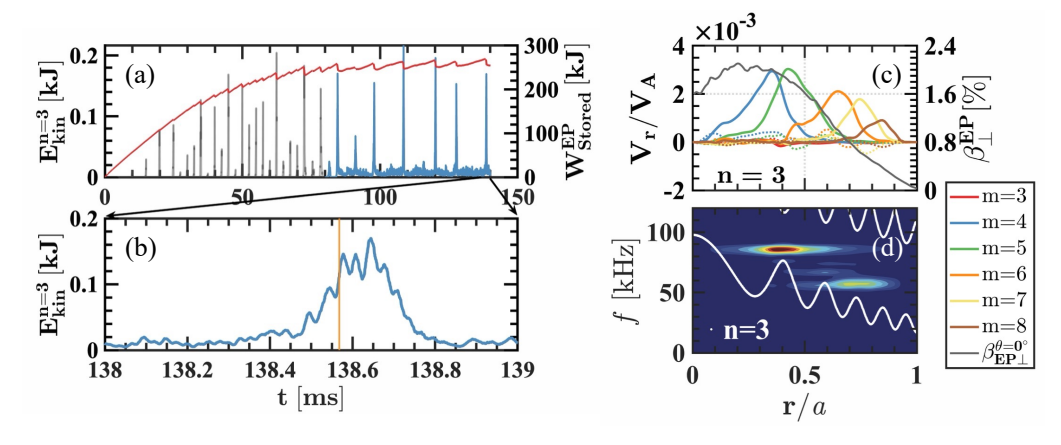


FIG. 6. Single-n simulation of ICRF-induced bursting event with an ICRF resonance layer located at the magnetic axis and an absorbed ICRF power of 6MW. (a) Evolutions of MHD kinetic energy and minority ion stored energy. (b) Zoomed MHD kinetic energy evolution of one bursting event. (c,d) Spatial profiles and frequency spectra of radial MHD velocity fluctuations at t=138.56ms.

3.4. Comprehensive simulation of non-bursting shear Alfvén waves

We further conducted comprehensive simulations of ICRF heating with an ICRF resonance layer located at the outboard side at the magnetic field of $B_0 = 1.5$ T. Two runs were conducted with an ICRF power of 6MW and 18MW, respectively. Figure 7(a,c) shows the evolution of MHD kinetic energy, minority ion stored energy. During the multi-phase period, the free energy stored in a short classical simulation interval of 0.5ms will lead to significant overshoots in MHD fluctuations in the following hybrid simulation. In the continuous hybrid simulation phase, TAEs are non-bursting for both cases. We performed continuous hybrid simulations over 20ms to confirm this nonlinear state. The total steady-state minority ion stored energy in the case of 6 MW is similar to the on-axis heating case shown in Figure 2. In the outboard ICRF heating, due to the smaller plasma volume in which minority ions reside, the maximum minority ion beta reaches almost double that of the bursting one. It is also noted that the majority of minority ions remain in a region close to the RF resonance layer. Therefore, resonant particles interacting with SAWs will also easily experience the strong RF-induced velocity space diffusion.

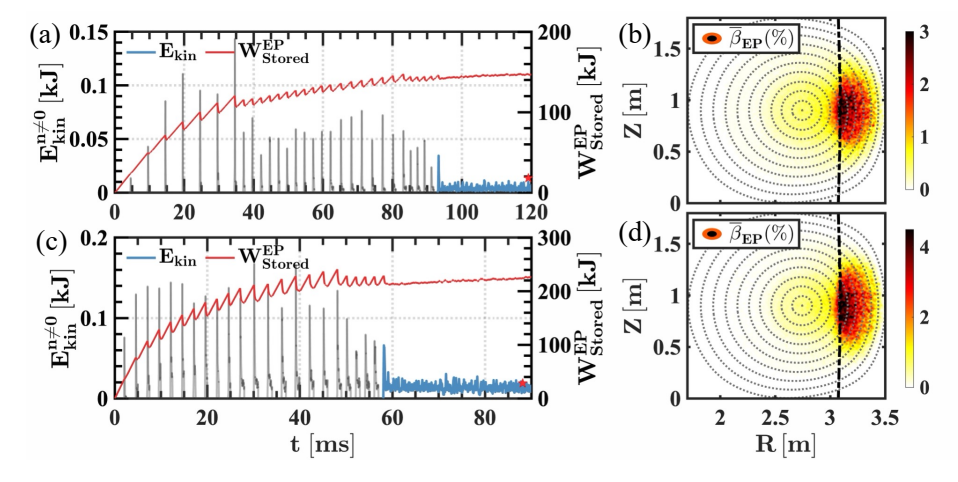


FIG. 7. Multi-phase simulation of ICRF-induced non-bursting event for absorbed RF power of 6MW (top) and 18MW (bottom) with an ICRF resonance layer located at r/a=0.4 of the outer equatorial plane. (a,c) Evolutions of MHD kinetic energy and minority ion stored energy, where the continuous hybrid simulation starts from t=93ms and t=58ms, respectively. (b,d) Steady-state minority ion beta profile in a cross-section.

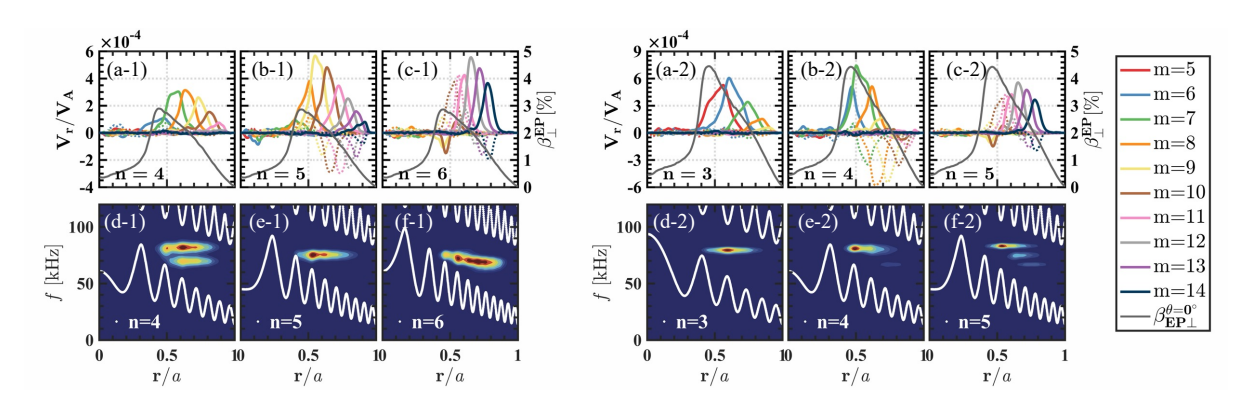


FIG. 8. Spatial profiles and frequency spectra of radial MHD velocity fluctuations of the non-bursting events shown in Fig. 7. Left panels show the fluctuations at t=119.13ms under an absorbed RF power of 6MW, while right panels show the fluctuations at t=88.16ms under a high RF power of 18MW.

Figure 8 shows the spatial profiles and the frequency spectra of the non-bursting modes. For the case with an absorbed RF power of 6MW, primary SAWs of each toroidal mode show a broad structure, composed of multiple TAEs with almost identical frequency. The RF-induced strong velocity space diffusion prevents continuous particle trapping in the radial direction and contributes to the formation of this broad structure with uniform mode frequency. The broad structure extends over more than 40% of the minor radius. Such a long-lasting broad structure will prevent the accumulation of free energy to trigger a bursting event. Moreover, two discrete modes of n=4 overlap radially in space. Consequently, it is no longer a prerequisite for these two discrete instabilities

to first grow independently to a significant amplitude to interact. For the case of 18 MW, the minority ion perpendicular beta remains at a value above 4%. Dominant unstable modes of n = 3, 4, 5 have a similar frequency and are all peaked between 0.5 and 0.6 minor radius. However, the mode amplitudes are not obviously enhanced. Besides, very weak discrete mode structures can be observed for n = 4 and n = 5 toroidal harmonics. Almost no discernible discrete structure was observed for the low toroidal mode number n = 3 during the entire continuous hybrid simulation phase.

4. SUMMARY AND CONCLUSION

To conclude, state-of-the-art hybrid particle-in-cell simulations of ICRF-induced TAEs in tokamak plasmas have been conducted, where SAW-induced fast-ion transport is self-consistently included during the high-energy tail formation. Both ICRF-induced bursting and non-bursting toroidal Alfvén eigenmodes (TAEs) are observed in a relatively low magnetic field $B_0 = 1.5$ T. Specifically, bursting TAEs occur when an ICRF resonance layer is located at the magnetic axis or inboard side, while the outboard heating always leads to non-bursting TAEs, regardless of RF power. The formation of discrete TAEs in radial space, but coherent in frequency space, plays a pivotal role in triggering the bursting event. It is further identified that the RF-wave-induced strong velocity space diffusion can prevent the formation of the discrete structures.

Although the present study diverges from previous works [15,16] in several key aspects, such as the driving mechanism (ICRF versus NBI), the topology of resonant particle orbits (trapped versus passing), the mode dynamics (fixed frequency versus chirping), and the synergetic type (radially discrete modes with the same n versus different n modes), they share an identical fundamental triggering mechanism. That is resonance overlap in phase space. Moreover, a process is necessary to suppress overlap formation for storing sufficient free energy. Therefore, the destruction of the coherent structure by scrambling resonant particles through fast-ion phase space engineering via RF waves could be a desirable strategy in preventing the bursting SAWs.

ACKNOWLEDGEMENTS

Numerical simulations were performed on the Plasma Simulator (NECSX-Aurora TSUBASA) of NIFS with the support and under the auspices of the NIFS Collaboration Research program (NIFS22KIST001), the Supercomputer Fugaku of the RIKEN Center for Computational Science (Project ID: hp220165, hp230113), the JFRS-1 of the International Fusion Energy Research Centre, and the Wisteria/BDEC-01 of the University of Tokyo. This work was supported by JSPS KAKENHI Grant Number JP21H04973 and JP24K17032, the NINS program of Promoting Research by Networking among Institutions (Grant Number 01422301), and MEXT as a Program for Promoting Research on the Supercomputer Fugaku (Exploration of burning plasma confinement physics, JPMXP1020200103).

REFERENCES

- [1] WONG, K.L., FONCK, R.J., PAUL, S.F. *et al.*, Excitation of Toroidal Alfvén Eigenmodes in TFTR, Phys. Rev. Lett., **66** 14 (1991) 1874-1877.
- [2] OSAKABE, M., et al., Experimental observations of enhanced radial transport of energetic particles with Alfvén eigenmode on the LHD, Nucl. Fusion 46 10 (2006) S911-S917.
- [3] SHINOHARA, K., et al., Alfvén eigenmodes driven by Alfvénic beam ions in JT-60U, Nucl. Fusion 41 5 (2001) 603-612.
- [4] GARCIA-MUNOZ, M., HICKS, N., VAN VOORNVELD, R., et al., Convective and Diffusive Energetic Particle Losses Induced by Shear Alfvén Waves in the ASDEX Upgrade Tokamak, Phys. Rev. Lett., **104** 18 (2010) 185002
- [5] KAZAKOV, YE. O., ONGENA, J. WRIGHT, J.C. *et al.*, Efficient generation of energetic ions in multi-ion plasmas by radio-frequency heating, Nat. Phys., **13** 10 (2017) 973–978.
- [6] WANG, J., TODO, Y., SEKI, R. et al., FEC 2023, London, U.K., Oct 16–21, 2023. Paper number IAEA-CN-316-1705.
- [7] FASOLI, A., BREIZMAN, B.N., BORBA, D. *et al.*, Nonlinear Splitting of Fast Particle Driven Waves in a Plasma: Observation and Theory, Phys. Rev. Lett., **81** 25 (1998) 5564-5567.

- [8] HEETER, R., FASOLI, A., SHARAPOV, S., Chaotic Regime of Alfvén Eigenmode Wave-Particle Interaction, Phys. Rev. Lett., **85** 15 (2000) 3177-3180.
- [9] BERK, H.L., BREIZMAN, B.N., PEKKER, M., Nonlinear Dynamics of a Driven Mode near Marginal Stability, Phys. Rev. Lett. **76** 8 (1996) 1256-1259.
- [10] BREIZMAN, B. N., BERK, H. L., PEKKER, M. S., Critical Nonlinear Phenomena for Kinetic Instabilities Near Threshold, Phys. Plasmas, 4 5 (1997) 1559-1568
- [11] LILLEY, M., BREIZMAN, B. N., SHARAPOV, S. E., Destabilizing Effect of Dynamical Friction on Fast-Particle-Driven Waves in a Near-Threshold Nonlinear Regime, Phys. Rev. Lett., **102**, 195003 (2009).
- [12] TODO, Y., BERK, H. L., BREIZMAN, B. N., Simulation of intermittent beam ion loss in a Tokamak Fusion Test Reactor experiment, Phys. Plasmas, 10 7 (2003) 2888-2902
- [13] LANG, J., FU, G. Y., CHEN, Y., Nonlinear Simulation of Toroidal Alfvén Eigenmode with Source and Sink, Phys. Plasmas, 17 4 (2010) 042309
- [14] TODO, Y., VAN ZEELAND, M.A., BIERWAGE, A., HEIDBRINK, W.W., Multi-Phase Simulation of Fast Ion Profile Flattening due to Alfvén Eigenmodes in a DIII-D Experiment, Nucl. Fusion, **54** 10 (2014) 104012.
- [15] TODO, Y., Critical Energetic Particle Distribution in Phase Space for the Alfvén Eigenmode Burst with Global Resonance Overlap, Nucl. Fusion, **59** 9 (2019) 096048.
- [16] BIERWAGE, A., SHINOHARA, K, TODO, Y. *et al.*, Simulations Tackle Abrupt Massive Migrations of Energetic Beam Ions in a Tokamak Plasma, Nat. Commun., **9** 1 (2018) 3282.
- [17] STIX, T.H., Fast-wave Heating of a Two-Component Plasma, Nucl. Fusion 15 5 (1975) 737.
- [18] MURAKAMI, S., et al., A Global Simulation Study of ICRF Heating in the LHD, Nucl. Fusion 46 7 (2006) S425-S432.
- [19] CHARLES, F.F. KARNEY, Fokker-Planck and Quasilinear Codes, Comput. Phys. Rep. 4 3-4 (1986) 183-244.
- [20] TODO, Y., BERK, H.L., BREIZMAN, B.N., Nonlinear Magnetohydrodynamic Effects on Alfvén Eigenmode Evolution and Zonal Flow Generation, Nucl. Fusion, **50** 8 (2010) 084016.